Crustal anatexis and melt extraction during deformation in the restitic xenoliths at El Joyazo (SE Spain)

B. CESARE

Dipartimento di Mineralogia e Petrologia, Università di Padova, Corso Garibaldi 37, I-35137 Padova, Italy

E. SALVIOLI MARIANI

AND

G. VENTURELLI

Istituto di Petrografia, Università di Parma, Viale delle Scienze 78, I-43100 Parma, Italy

Abstract

The dacite of El Joyazo contains abundant metapelitic xenoliths. These can be divided into two main types: garnet–biotite–sillimanite and spinel–cordierite xenoliths. In the xenoliths the widespread occurrence of rhyolitic glass as interstitial films, foliation-parallel layers and primary melt inclusions in all mineral phases indicates that these assemblages developed in the presence of a melt phase, i.e. during anatexis. The composition of the interstitial glass is comparable to that of the melt inclusions, suggesting that melt was locally produced. Phase equilibria indicate that anatexis occurred at $P-T$ conditions of 5–7 kbar and 850 ± 50°C.

Several microstructural lines of evidence show that melt extraction was assisted by deformation during foliation development, and that on the scale of the xenoliths (up to 50 cm) melt escaped mainly by flow along foliation planes. The development of a *syn-anatectic* foliation also suggests that metapelitic rocks were involved in high-grade metamorphism and partial melting prior to fragmentation and dispersion in the host dacite.

Mass balance calculations, based on the chemical composition of interstitial glass and melt inclusions in minerals, the bulk xenoliths and representative samples of potential pelitic sources support a model wherein the xenoliths represent restites after the extraction of 30 to 55 wt.% melt from graphitic metapelite protoliths similar to the rocks constituting the surrounding Alpujarride metamorphic complex.

KEYWORDS: anatexis, deformation, glass, metapelite, microstructures, Spain, xenoliths.

Introduction

PARTIAL melting of crustal rocks is one of the main mechanisms of production of granitoid magmas. Thus, it is important to characterize the various aspects of this process, such as the chemistry and amount of melt produced as a function of the geodynamic regime and type of protolith, the mode of segregation of melt from the parent rocks and the mechanisms of ascent and emplacement of melt at higher crustal levels.

Field-based studies of anatectic processes are generally performed in migmatitic complexes from granulitic terranes (e.g. Grant and Frost, 1990; Srogi *et al.*, 1993). In this case the leucocratic material is considered (or demonstrated) to represent the former melt, which was segregated from the adjacent parent rock. An alternative option for the study of anatexis is experimental investigation using well characterized chemical systems, under controlled P and T conditions (e.g. Johnston and Wyllie, 1988; Vielzeuf and Holloway, 1988; Holtz and Johannes, 1991;

Mineralogical Magazine, Vol. 61, February 1997, pp. 15–27

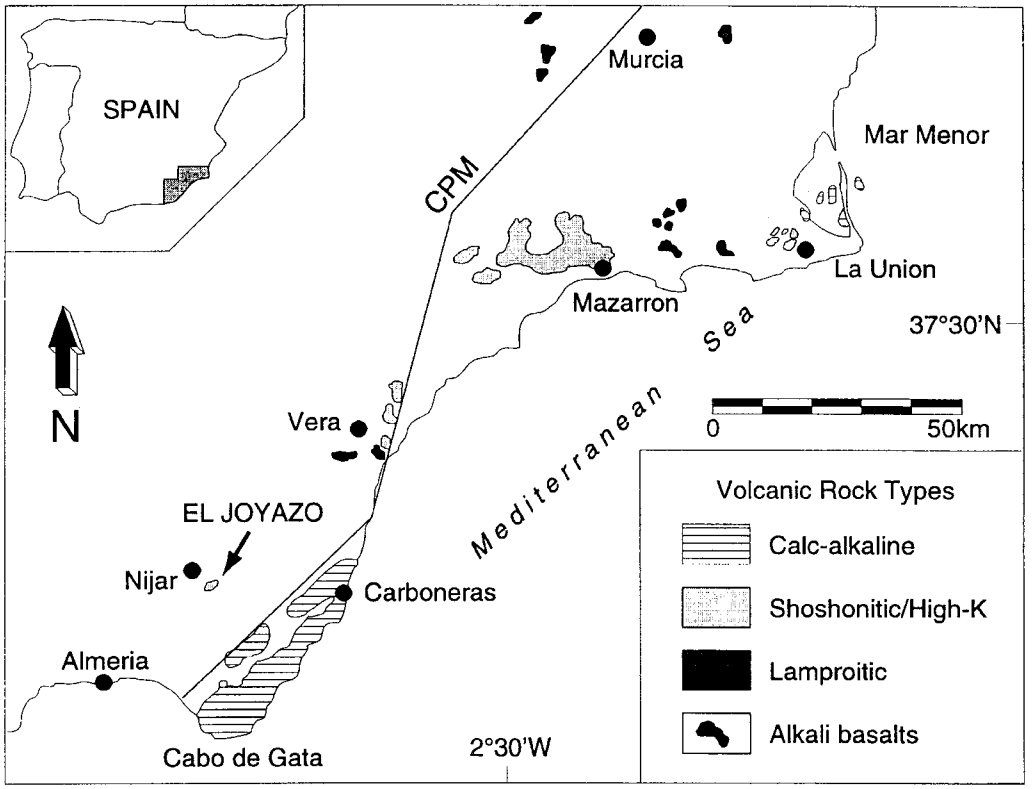

FIG. 1. Sketch map of the Miocene volcanic rocks outcropping in SE Spain (modified after Lopez Ruiz and Rodriguez Badiola, 1980). CPM: Carboneras-Palomares-Alhame de Murcia Fault System.

Patiño Douce and Johnston, 1991; Vielzeuf and Montel, 1994).

Unfortunately, in both cases the information obtained on the actual processes of melting and melt segregation, and on the role of deformation, is incomplete. Migmatitic rocks commonly undergo extensive (re)crystallization as well as textural and chemical reequilibration in response to slow cooling; on the other hand, experimental petrology in general does not give significant textural information applicable to natural conditions.

A more straightforward investigation of the mechanisms of partial melting is sometimes possible in cases where partially molten crustal fragments are rapidly transported to the Earth's surface as xenoliths in lava flows (e.g. Hayob *et al.*, 1989). In this case, the crustal xenoliths are rapidly cooled, and any melt derived from anatexis is preserved as glass within the restitic assemblage.

An example of this scenario is offered by the metapelitic xenoliths hosted by the dacitic lava of El Joyazo, SE Spain (Zeck, 1970). Due to the abundance of glass present and the deformation textures, these rocks have been studied in order to characterize, at a small (mm-dm) scale, the process of melt extraction during deformation.

Geologic setting

During the Miocene, from about 15 to 6 Ma (Nobel *et al.* 1981; Bellon *et al.*, 1983; Di Battistini *et al.*, 1987), an intense calc-alkaline to lamproitic magmatism developed in the eastern portion of the Betic Cordillera, SE Spain (Lopez Ruiz and Rodriguez Badiola, 1980; Toscani *et al.*, 1990; Fig. 1). In the same area, a fault system (Carboneras-Palomares-Alhame de Murcia Fault System) was active as sinistral strike-slip faults at least since the Late Miocene, leading to the juxtaposition of disparate crustal segments. To the east of this fault system the lithosphere is thinner (about 22 km thick), denser and characterized by higher heat flow values than to the

west; this indicates a mantle thermal anomaly under the area of thinner crust (De Larouzière *et al.*, 1988 and references therein).

Outcrops of calc-alkaline to shoshonitic rocks are widespread along the fault system, in an area from Mar Menor in the NE to the depression of Nijar, close to Almeria, in the SW (Lopez Ruiz and Rodriguez Badiola, 1980). The few available geochronological data on these rocks suggest an age of about 6.5–8.5 Ma. With few exceptions, all of the rocks of Mar Menor, La Union, Mazarron and Vera are corundum-normative and commonly contain variable amounts of magmatic and metapelitic xenoliths. In places xenoliths are very abundant, such as at El Joyazo, NE of Almeria.

The volcanic edifice of El Joyazo formed during the Messinian as a small extrusion, later covered by a coral reef. At present, the volcanic structure is deeply eroded, forming a crater-like depression. The fine-grained volcanic rocks consist of a rhyolitic, glassy groundmass containing phenocrysts (<l mm) of biotite, plagioclase, clino- and ortho-pyroxene, amphibole and sector-twinned cordierite. Moreover, the rock contains isolated mineral grains of garnet, biotite, hercynitic spinel, sillimanite, cordierite and rounded quartz and polycrystalline fragments that represent dismembered metapelitic xenoliths. The bulk rock, inclusive of its relevant xenocryst fraction, can be described as dacite (Table 1).

Petrographic and isotopic (Sr, O) data on the dacite and its xenoliths are reported by Zeck (1968, 1970) and Munskgaard (1984, 1985). Both authors interpret the dacitic magma and the metamorphic xenoliths as syngenetic products of the anatexis of semipelitic rocks, where the dacite represents the contaminated granitoid melt and the metamorphic xenoliths the Al-rich restitic portion.

The metapelitic xenoliths

Two main types of metapelitic xenoliths occur in the dacite, garnet–biotite–sillimanite (Grt–Bt–Sil) and spinel–cordierite (Spl–Crd) xenoliths. The quartz–cordierite rocks, distinguished by Zeck (1970) as a further xenolith type, are actually the products of interaction between Grt–Bt–Sil xenoliths and blebs of mafic magma (Salvioli Mariani *et al.*, 1995), and are not considered in this study.

Grt–Bt–Sil xenoliths. These xenoliths are the most abundant inclusions in the dacite. They are characterized by a medium to coarse grain-size of the matrix and garnet porphyroblasts up to 1 cm in diameter (Fig. 2*a*). These xenoliths can reach a maximum length of 60 cm. In hand specimen, a weak stretching lineation and a faint schistosity, marked by the alternation of biotite and sillimanite folia, can be observed. The common assemblage includes biotite, fibrous sillimanite, almandine garnet, plagioclase (anorthite 25–35%), graphite, apatite, glass, ± ilmenite, ± cordierite, ± hercynitic spinel, ± quartz (Tables 2 and 3).

Spl–Crd xenoliths. This rock type is fine-grained, with euhedral porphyroblasts of hercynitic spinel reaching a maximum size of 2 mm; it shows a well-

TABLE 1. Chemical composition of dacitic lavas and metapelitic xenoliths from El Joyazo, and of graphitic phyllite and mica schist of the Alpujarride metamorphic complex.

	Dacitic lavas		Grt-Bt-Sil xenoliths		Crd-Spl xenoliths		Phyllite	Mica schist
	(11)	range	(5)	range	(6)	range	(1)	(1)
SiO_2	63.2	62.0–64.1	44.2	43.0–45.1	40.0	37.7–42.0	58.6	56.7
TiO_2	0.62	0.59–0.70	1.68	1.60–1.85	1.87	1.73–2.04	0.90	1.11
Al_2O_3	17.0	16.1–17.4	31.6	30.0–32.8	34.3	31.4–38.0	21.2	22.8
Fe_2O_3*	4.78	4.30–5.32	10.1	9.44–10.9	14.1	12.6–14.8	5.68	8.67
MnO	0.05	0.04–0.06	0.07	0.04–0.12	0.16	0.12–0.18	0.03	0.10
MgO	1.98	1.59–2.40	2.64	2.45–2.80	3.25	2.86–4.27	1.71	1.67
CaO	2.58	2.30–2.88	1.44	0.91–1.81	1.32	0.39–4.70	0.53	0.37
Na_2O	2.16	2.04–2.36	1.71	1.15–2.21	0.73	0.30–1.73	1.09	1.02
K_2O	3.50	3.09–3.80	3.88	3.49–4.50	2.40	0.76–4.18	4.24	3.63
P_2O_5	0.17	0.14–0.19	0.22	0.11–0.35	0.12	0.06–0.18	0.20	0.12
L.O.I.	4.22	3.25–5.30	2.48	1.76–3.30	1.97	0.25–2.88	5.09	4.16
Total	99.96		100.02		100.22		99.27	100.35

Analyses have been performed by X-ray fluorescence on glass discs. (n) = average composition of n samples.
* Total Fe as Fe_2O_3

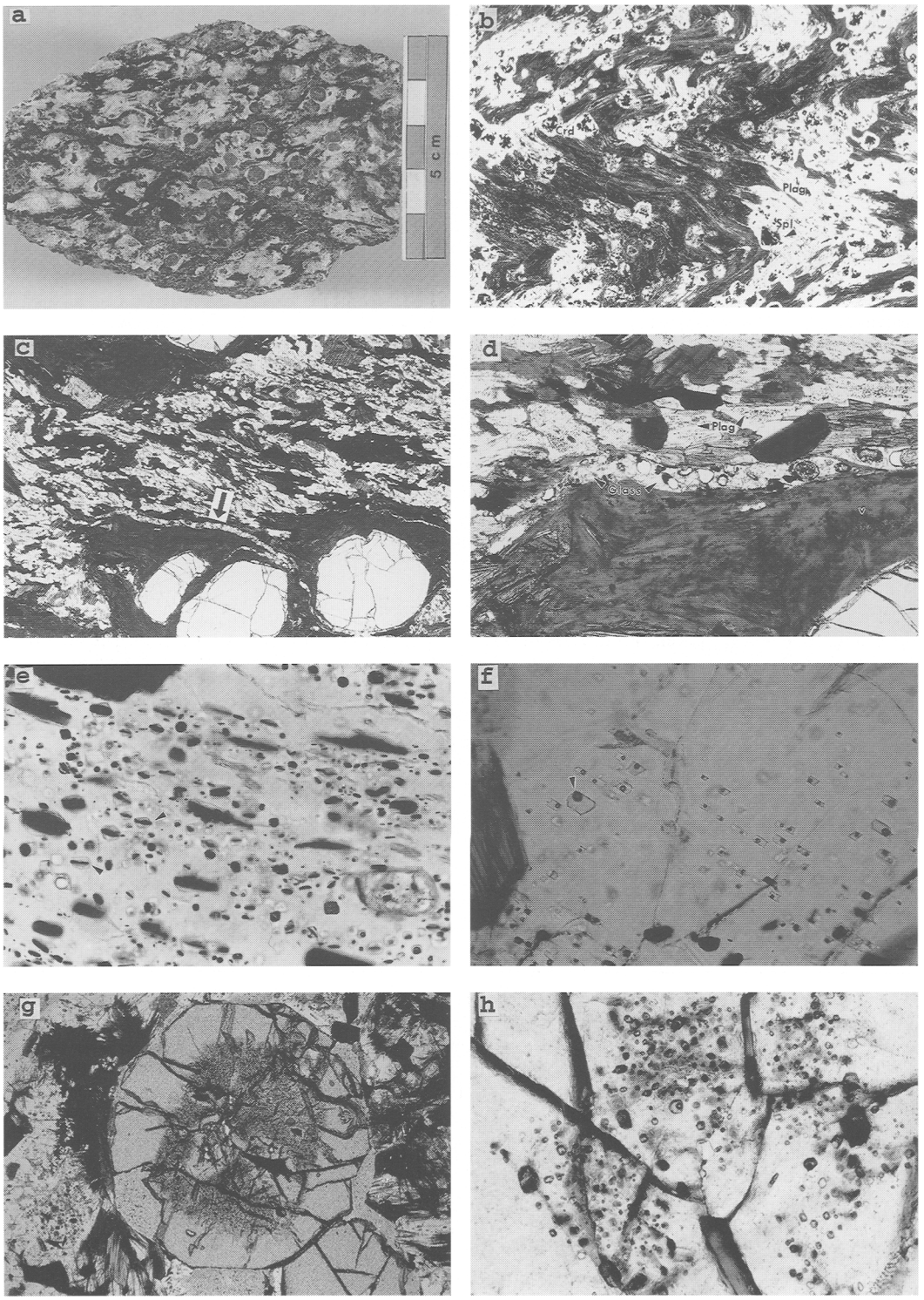
a
5 cm
b
Crd
Plag
Spl
c
d
Plag
Glass
e
f
g
h

TABLE 2. Mineral assemblages of the metapelitic xenoliths

	Grt-Bt-Sil xenoliths					Spl-Crd xenoliths			
	SP 819d	SP 823	SP 829	HO 04a	HO 33a	SP 832	HO 19	HO 27	HO 31
Apatite	X	X	X	X	X				
Biotite	X	X	X	X	X	X	X	X	X
Calcite			X						
Cordierite	X				X	X	X	X	X
Corundum						X			
Garnet	X	X	X	X	X		X	X	X
Glass	X	X	X	X	X	X	X	X	X
Graphite	X	X	X	X	X	X	X	X	X
Hercynite				X	X	X	X	X	X
Ilmenite	X			X	X	X	X	X	X
K-feldspar							X	X	
Plagioclase	X	X	X		X	X	X	X	X
Quartz	X*							X	
Sillimanite	X	X	X	X	X	X	X	X	X

* Armoured relic

developed, closely-spaced, folded foliation (Fig. 2*b*). The mineral composition is more complex than in the Grt–Bt–Sil xenoliths, and includes biotite, cordierite, sillimanite, hercynitic spinel, graphite, ilmenite, glass, ± almandine garnet, ± plagioclase (anorthite 45%), ± quartz, ± sanidine, ± corundum.

Some important features are common to both types of xenolith:

(*a*) Glass of rhyolitic composition (Table 4) is present as foliation-parallel layers reaching a maximum thickness of about 100 μm (Fig. 2*c, d*) as thin films coating garnet and spinel porphyroblasts, and as inclusions (Fig. 2*e–h*) in almost all minerals (garnet, biotite, spinel, ilmenite, plagioclase, cordierite, corundum, sillimanite, apatite, monazite). The melt inclusions range in size from a few to 50 μm, and the largest ones generally occur within plagioclase (Fig. 2*f*). Most inclusions (Fig. 2*g*) fulfill the textural requirements for a primary trapping, i.e. for formation during the growth of the mineral host (Roedder, 1984). The widespread occurrence of primary glass inclusions within *all* minerals is evidence that the xenoliths underwent a (re)crystallization in the presence of a melt phase, i.e. during anatexis.

(*b*) The xenoliths do not contain quartz, except for rare, small grains that occur as armoured relics within garnet or plagioclase. This suggests that further progress of the partial melting process may have been inhibited by quartz exhaustion.

(*c*) Graphite is always abundant, and occurs either as large flakes in the biotite–sillimanite layers or as

FIG. 2. (*a*) Polished surface of a Grt–Bt–Sil xenolith, showing the well developed biotite–sillimanite cleavage and garnet porphyroblasts. (*b*) Folded cleavage, marked by sillimanite-rich folia, in a Spl–Crd xenolith. Dark crystals are hercynitic spinel, statically overgrowing the folded foliation; white crystals, often armouring hercynite, are cordierite and plagioclase. Width of view: 8.7 mm. (*c*) One glass layer (arrow) parallel to the foliation that anastomoses around garnet porphyroblasts and sillimanite-melt knots. The white matrix is composed of plagioclase. Grt–Bt–Sil xenolith, width of view: 3.4 mm. (*d*) Enlarged view of the glass layer. Plagioclase crystals contain abundant inclusions of graphite and rhyolitic glass. Width of view: 0.67 mm. (*e*) Abundant, randomly distributed glass inclusions in a crystal of plagioclase. Most glass inclusions in this sample contain a small plate of graphite (black, arrows), also occurring as solid inclusions in the plagioclase. Glass inclusions commonly exhibit a negative crystal shape. Grt–Bt–Sil xenolith, width of view: 1.35 mm. (*f*) Glass inclusions in a crystal of plagioclase. The small bubble within the glass inclusions (arrow) is the 'shrinkage bubble' and is empty. No fluid inclusions were observed in this sample. Grt–Bt–Sil xenolith, width of view: 0.67 mm. (*g*) Garnet porphyroblast in a Grt–Bt–Sil xenolith. The dark core is rich in glass inclusions (enlarged in the next figure). The zonal distribution of inclusions is an indication for primary trapping (Roedder, 1984; p. 18). Width of view: 3.4 mm. (*h*) Close up of a porphyroblast of garnet rich in randomly distributed glass inclusions. Width of view: 0.50 mm.

TABLE 3. Electron microprobe analyses of mineral phases from xenoliths and lava

Sample	HO 04	HO 19	HO 832	HO 832	HO 31	HO 33a	HO 27	HO 823	HO 31	HO 33a	HO 31	SP 832
Rock type	Grt-Bt-Sil	Spl-Crd	lava	Grt-Bt-Sil	Spl-Crd	Grt-Bt-Sil	Spl-Crd	Grt-Bt-Sil	Spl-crd	Grt-Bt-Sil	Spl-crd	lava
Phase	Her	Her	Crd	Crd	Crd	Bt	Bt	Grt	Grt	Pl	Pl	Pl
SiO_2	0.00	0.04	47.27	49.11	46.51	34.09	34.63	37.11	37.36	60.76	57.83	48.53
TiO_2	0.38	0.18	0.00	0.03	0.02	5.03	6.53	0.02	0.16	0.02	0.04	0.04
Al_2O_3	57.26	57.80	32.41	32.47	32.30	18.48	16.93	20.83	20.87	24.79	26.39	32.76
Fe_2O_3*	2.90	2.48										
FeO	32.50	35.06	12.51	10.58	12.78	23.09	20.45	36.80	35.42	0.09	0.13	0.20
MnO	0.10	0.12	0.08	0.21	0.04	0.05	0.05	1.81	1.67	0.01	0.01	0.05
MgO	5.06	3.28	5.95	7.39	5.58	6.35	7.75	3.14	3.86	0.01	0.00	0.00
Na_2O			0.19	0.09	0.08	0.48	0.41	0.91	1.06	7.34	5.64	2.06
K_2O			0.14	0.10	0.21	8.38	8.76			0.81	1.10	0.09
CaO	0.00	0.00	0.04	0.05	0.06	0.01	0.00			6.26	8.76	16.77
ZnO	0.79	1.41										
Total	98.99	100.37	98.59	100.03	97.58	95.96	95.52	100.62	100.40	100.10	99.89	100.50
Si	0.000	0.001	4.960	5.025	4.974	5.240	5.300	5.976	5.985	2.703	2.599	2.215
Ti	0.008	0.004	0.000	0.002	0.001	0.581	0.751	0.002	0.019	0.001	0.001	0.001
Al	1.922	1.937	4.008	3.916	3.997	3.348	3.054	3.953	3.941	1.300	1.397	1.762
Fe^{2+}	0.774	0.834	1.098	0.905	0.991	2.967	2.617	4.957	4.746	0.003	0.005	0.008
Fe^{3+}*	0.062	0.053										
Mn	0.002	0.003	0.007	0.018	0.012	0.006	0.007	0.247	0.228	0.000	0.000	0.002
Mg	0.215	0.139	0.930	1.127	1.033	1.456	1.769	0.754	0.922	0.000	0.000	0.000
Ca	0.000	0.000	0.005	0.005	0.004	0.001	0.000	0.157	0.182	0.298	0.422	0.820
Na			0.038	0.018	0.013	0.144	0.121			0.633	0.491	0.183
K			0.018	0.013	0.015	1.644	1.711			0.046	0.063	0.005
Zn	0.017	0.030										
Oxygens	3	3	18	18	18	20	20	24	24	8	8	8
Mg/(Mg+Fe)	0.22	0.14	0.46	0.55	0.51	0.33	0.40	0.13	0.16			
Anorthite										32%	46%	82%

Analyses have been performed with a CAMECA Camebax electron microprobe at the C.N.R. laboratory of the Department of Mineralogy and Petrology of Padova University.

* Recalculated assuming charge balance.

TABLE 4. Electron microprobe* analyses of interstitial glass and glass inclusions in the xenoliths and of groundmass glass in the host dacite of El Joyazo

	Grt-Bt-Sil xenoliths					
	in garnet		in plagioclase		interstitial	
	(5)	range	(6)	range	(7)	range
SiO_2	71.6	69.3–74.0	72.8	71.6–73.5	69.9	68.0–71.6
TiO_2	0.06	0.05–0.08	0.05	0.00–0.10	0.14	0.00–0.21
Al_2O_3	13.8	12.6–14.4	12.9	12.0–13.4	14.8	12.5–15.6
Fe_2O_3**	1.84	1.44–2.15	1.18	0.99–1.40	2.05	1.75–2.16
MgO	0.06	0.00–0.10	0.19	0.11–0.28	0.20	0.00–0.29
CaO	0.64	0.11–1.28	0.17	0.11–0.26	0.74	0.44–0.90
Na_2O	2.78	2.14–3.36	2.46	2.15–3.15	2.30	2.13–3.51
K_2O	4.04	3.48–4.40	4.12	3.55–5.49	5.11	4.70–5.74
Total	94.82		93.87		95.24	
Al_2O_3/SiO_2	0.19	0.17–0.20	0.18	0.16–0.19	0.21	0.20–0.22
K_2O/Na_2O	1.5	1.3–1.6	1.7	1.5–2.4	2.2	2.0–2.6

	Crd-Spl xenoliths					Dacite	
	in ilmenite	in hercynite		interstitial		interstitial	
	(1)	(6)	range	(8)	range	(5)	range
SiO_2	71.2	69.9	68.0–73.1	71.8	69.3–73.1	73.7	72.7–74.5
TiO_2	0.45	0.12	0.00–0.31	0.18	0.07–0.24	0.08	0.00–0.18
Al_2O_3	14.7	14.2	12.6–15.3	13.5	12.4–14.7	12.2	11.3–12.7
Fe_2O_3**	1.93	2.53	1.81–3.41	2.06	1.33–3.03	1.85	1.63–2.05
MgO	0.00	0.14	0.00–0.31	0.10	0.02–0.23	0.12	0.00–0.35
CaO	1.23	1.48	0.54–1.95	0.97	0.84–1.24	0.38	0.00–0.50
Na_2O	2.62	3.02	2.55–3.65	2.58	2.00–3.00	2.10	1.79–2.43
K_2O	4.57	4.50	3.69–5.03	4.90	4.00–5.60	5.28	4.92–5.52
Total	96.70	95.89		96.09		95.71	
Al_2O_3/SiO_2	0.20	0.20	0.17–0.22	0.19	0.17–0.21	0.16	0.15–0.17
K_2O/Na_2O	1.7	1.5	1.1–2.0	1.9	1.8–2.0	2.6	2.2–3.1

* Na_2O has been anlysed by EDS microanalysis at the Institute of Petrography of Parma University. Working conditions of 15 kV and 0.62 nA were used to avoid Na volatilization.
** Total Fe as Fe_2O_3
(n) = average value of n analyses; 0.00 = not detected.

trails of fine-grained inclusions within most minerals, especially biotite and plagioclase, to define a closely spaced internal foliation. Thus, the protolith of the xenoliths is inferred to have been a graphite-rich metapelite. Given the absence of any mineralogical relic, the internal foliation described above represents the only indication for a metamorphic event(s) predating the partial melting of these metapelites.

Microstructures

Anatexis and recrystallization of the xenoliths produced distinctive textures among glass and mineral phases, as described below.

(*a*) Both xenolith types show the presence of a well developed main foliation, generally marked by subparallel crystals of biotite and graphite (and/or acicular sillimanite). Biotite flakes in this foliation commonly contain melt inclusions.

(*b*) In the Grt–Bt–Sil xenoliths, the main foliation anastomoses around garnet porphyroblasts containing glass inclusions, or around knots of acicular sillimanite immersed in interstitial melt (Fig. 3*a*, *b*).

(*c*) Relics of an earlier foliation can be observed in strain shadows around garnet (Fig. 4*a*) and within microlithons in the main foliation (Fig. 4*b*). The earlier foliation is generally marked by graphite and

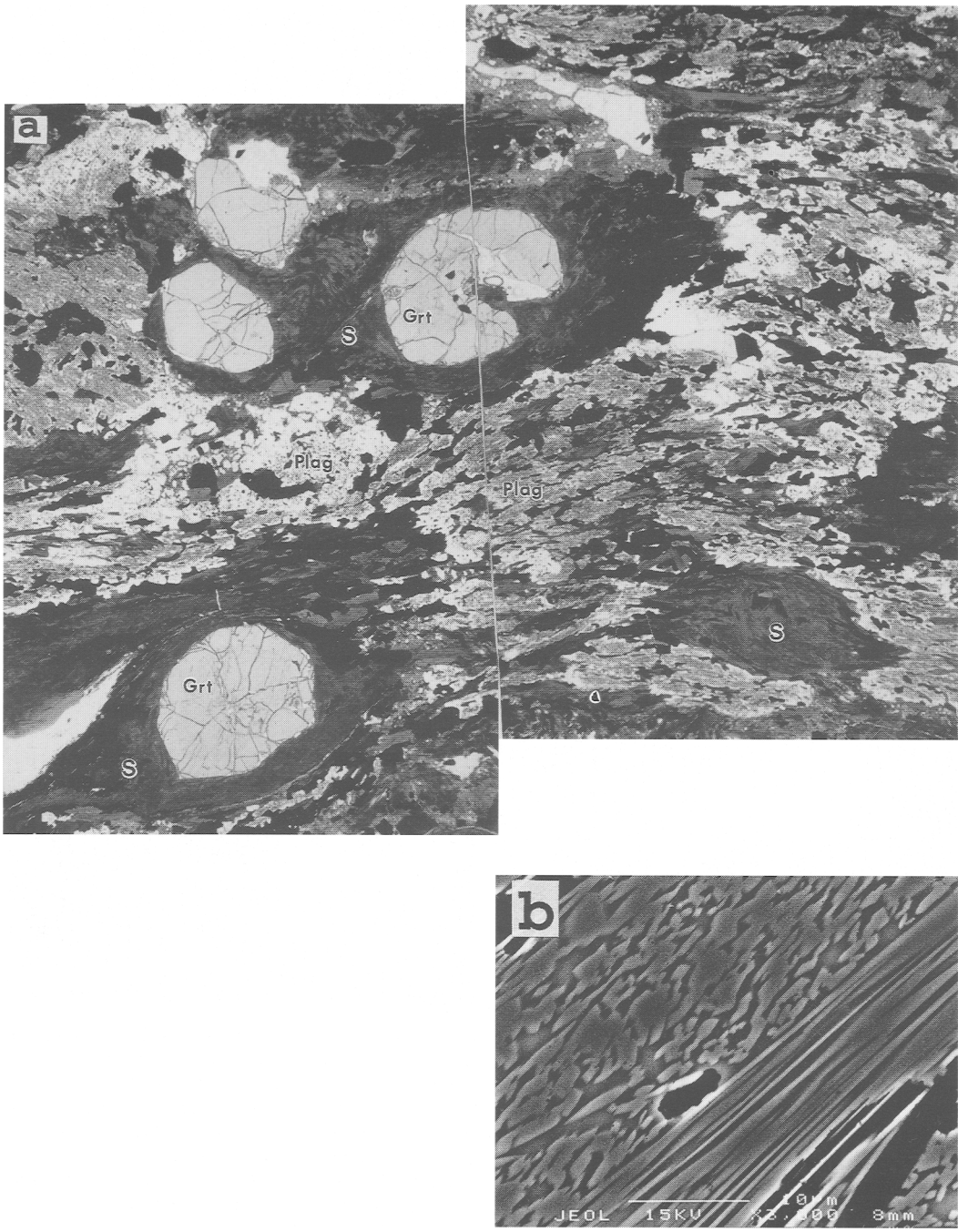

FIG. 3. (*a*) Grt–Bt–Sil xenolith: anastomosing of the main foliation around garnet porphyroblasts and sillimanite–glass knots (S) The rock matrix is mainly composed of plagioclase (white, dusty aspect owing to abundant glass inclusions) and biotite. Width of view: 15 mm. (*b*) SEM backscattered image of a nodule of sillimanite (lighter grey) plus melt (darker grey).

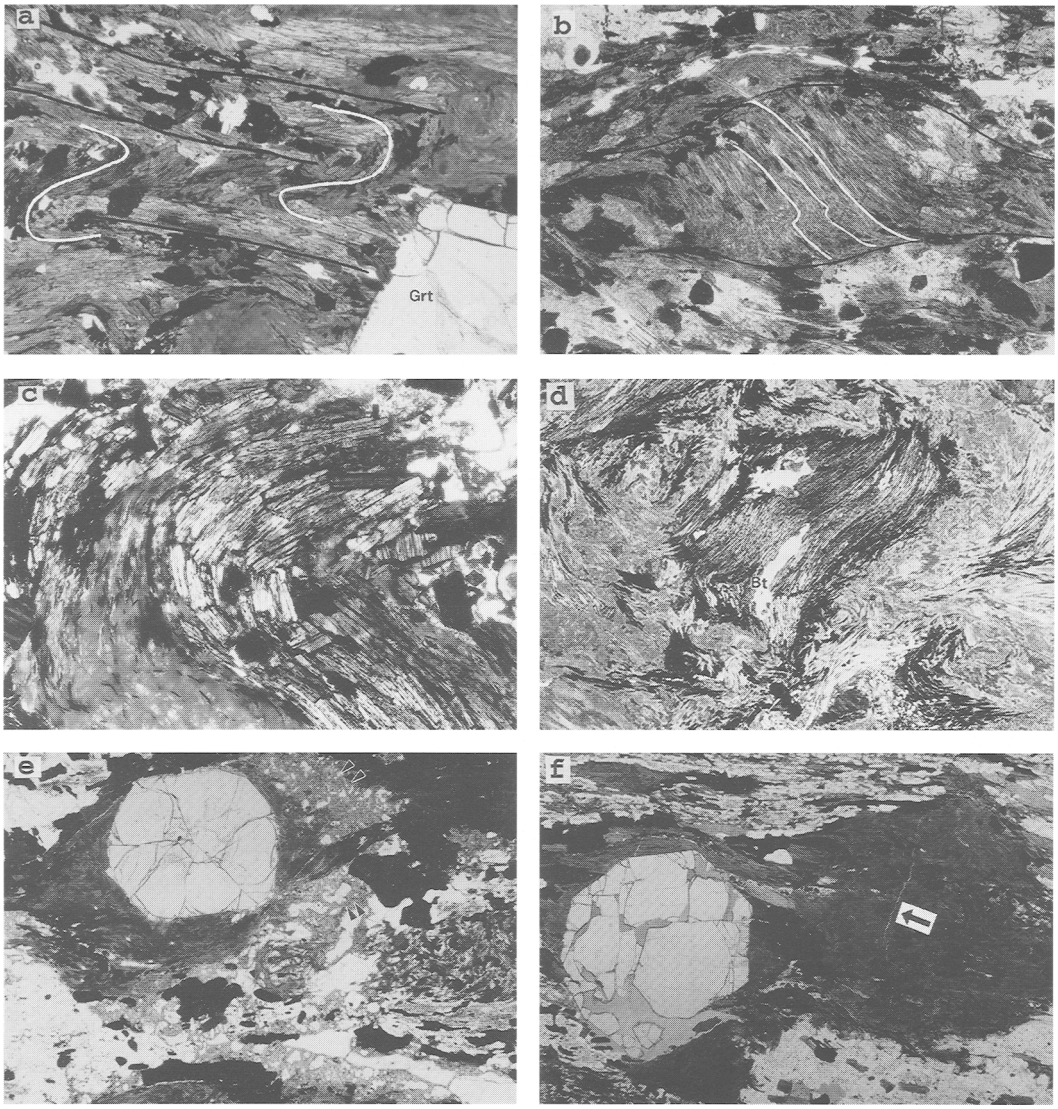

FIG. 4. (*a*) Strain-shadow around a porphyroblast of garnet preserving relics of an earlier, crenulated foliation (white) within the main foliation (black). Width of view: 2.1 mm. (*b*) Sillimanite–biotite microlithon wrapped by the main foliation (running E–W). The microlithon preserves a relict crenulation cleavage, well developed in the sillimanite–melt portion. Width of view: 3.4 mm. (*c*) Polygonal arc of biotite and graphite defining an earlier, folded foliation. Main foliation is oriented E–W in the picture. Width of view: 3.4 mm. (*d*) Bent crystal of biotite, preserving the earlier cleavage, within the E–W main foliation. Width of view: 3.4 mm. (*e*) Pockets of partly devitrified glass (arrows) in the strain shadow around a porphyroblast of garnet. Width of view: 8.7 mm. (*f*) Thin, glass- filled extensional fracture perpendicular to the main foliation (arrow). The fracture cuts across a sillimanite + melt knot, probably a pseudomorph after garnet. Width of view: 6.3 mm.

biotite, and is involved in both slight crenulation and isoclinal folding. Minerals in the earlier foliation also contain glass inclusions or are intergrown with glass. Crystals are generally undeformed in the microfolds and trace polygonal arcs (Fig. 4*c*); bent biotite flakes are rare (Fig. 4*d*).

(*d*) The interstitial rhyolitic glass preferentially occurs as thin layers parallel to the foliation (Fig. 2*c*, *d*) or in pockets in (or close to) strain shadows around garnet and sillimanite + glass knots (Fig. 4*e*). Glass has also been observed in rare, isolated, extensional fractures at a high angle to the foliation (Fig. 4*f*). These veinlets have a maximum thickness of 30 μm, and sometimes appear to be the result of boudinage. The lengths of the extensional fractures are always shorter than the associated foliation-parallel layers.

These microstructural features demonstrate that in both xenolith types the strain that produced the main foliation occurred in the presence of melt, during the partial melting of the metapelite. Moreover, the above relationships allow determination of the relative timing of partial melting of xenoliths and incorporation in the dacite. Since foliation development is synchronous with anatexis, and because stress transfer is inefficient within a liquid, it follows that the strain evident in the xenoliths, as well as the concomitant high-grade metamorphism and partial melting, must have all occurred before fragmentation and dispersion of the xenoliths in the host dacite.

Melt extraction

The glass occurring in the interstitial layers, in the inclusions, and in the groundmass of the dacite exhibits corundum-normative rhyolitic composition. The glass of the dacite, however, has an extreme composition characterized by the lowest Al_2O_3/SiO_2 and the highest K_2O/Na_2O ratios (Table 4). This suggests that the glass occurring in the xenoliths was not injected from the surrounding dacite during magma ascent. Furthermore, the presence, location and composition of the glass confirm the hypothesis of Zeck (1970) and Munskgaard (1984) who, based on geochemical arguments, interpreted these rocks as restites after melt extraction. During deformation, some of the rhyolitic melt was preserved as glass inclusions within mineral grains, and in the strain shadows around porphyroblasts or rigid mineral aggregates. The main physical processes of anatexis and melt extraction during deformation can be modelled as follows.

Protolith and amount of melt. In order to test the hypothesis that the graphitic metapelite protolith of the xenoliths belongs to the nearby Alpujarride basement of the Betic Cordillera, two fine-grained samples, a biotite–garnet phyllite and a garnet–staurolite–kyanite mica schist, were selected as model starting compositions.

Taking the bulk chemical composition of phyllite, mica schist, and xenoliths (Table 1), and the glass analyses (Table 4), mass-balance calculations show that these compositions are collinear in the Si-Al-Fe-Ti-Mg-K system (Fig. 5). This supports the hypothesis that the Grt–Bt–Sil xenoliths formed by

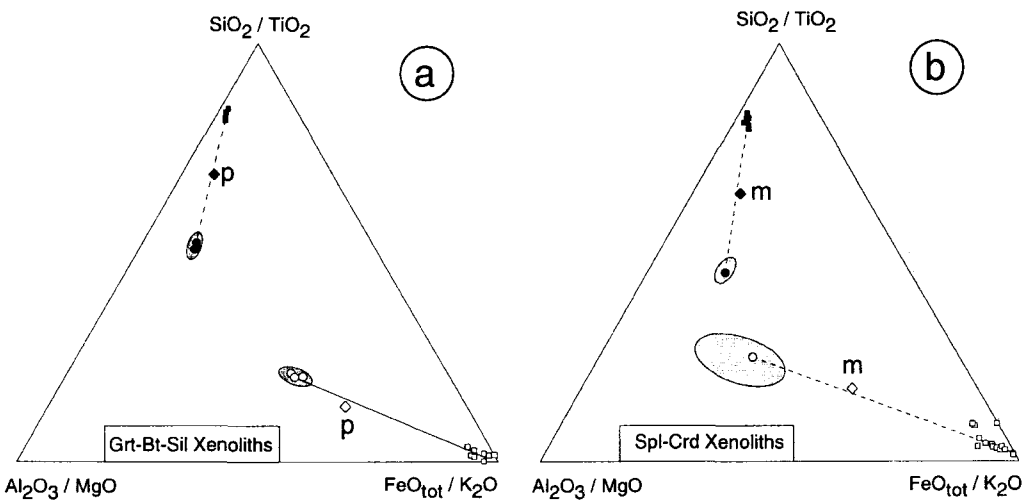

FIG. 5. Composite wt.% SiO_2–Al_2O_3–FeO_{tot} and TiO_2–MgO–K_2O ternary plots constructed with the chemical data of Tables 1 and 4. (*a*) Grt–Bt–Sil xenoliths; (*b*) Spl–Crd xenoliths. Filled symbols: SiO_2–Al_2O_3–FeO_{tot} system; empty symbols: TiO_2–MgO–K_2O system. Squares: glass analyses; diamonds: metapelites (m = micaschist, p = phyllite); circles: xenoliths. Shaded areas represent the compositional variations of the analysed xenoliths. Given the chemistry of xenoliths and glasses, dashed lines represent the possible composition for the protoliths. The analysed mica schist and phyllite of the Alpujarride basement plot along, or very close to, these lines. Degrees of melting can be estimated with the lever rule, and are in the range 35–55%.

extraction of 30(?)–60 wt.% rhyolitic melt from a metapelite with the composition of the analysed biotite–garnet phyllite, and the Spl–Crd xenoliths by extraction of about 40–55 wt.% melt from a composition similar to the analysed mica schist. These conclusions, however, are not supported by the distribution of Ca and Na, which puts limits on the model. Such inconsistency, that involves two oxides that sum to less than 5 wt.% of the rock total, may be related to variations (not determined by our sampling) in the plagioclase content of the metapelite protolith. Note that the actual degree of partial melting was higher, because glass is still present (often abundant) within the xenoliths.

Escape pathways. The abundance of melt inclusions within minerals, compared with the relative scarcity of layer-parallel or interstitial glass films, indicates that most of the melt was extracted during the deformation and recrystallization of the xenoliths, i.e. that melt segregation was deformation-assisted.

The interstitial glass occurs almost entirely as layers parallel to the cleavage and only very rarely as glass-filled fractures crosscutting the foliation. This suggests that: (i) at least on hand-specimen scale ($\sim$20 cm), melt escaped from the metapelites mainly by flow along foliation planes during ductile deformation; (ii) if a network of fractures was present to allow faster and more effective flow and collection of melt, its spacing was wider than the average size of xenoliths. Such a network may also have provided and controlled the surfaces of disaggregation of the partially molten rocks.

P–T conditions. Pressure and temperature conditions during partial melting have been evaluated using the Grt–Bt geothermometer (Ferry and Spear, 1978) and the geobarometers GASP (Newton and Haselton, 1981) and Grt–Crd (Aranovich and Podlesskii, 1983). For Grt–Bt–Sil xenoliths there is a good agreement of T values estimated in the different samples (Table 5) indicating that these rocks equilibrated at a temperature of 850 ± 50°C. The different barometers give comparable results of about 5–7 kbar.

The Spl–Crd xenoliths seem to have equilibrated at higher temperatures (up to 980°C) at similar pressure conditions (4–7.5 kbar).

The calculated temperatures, although in agreement with the large melt fractions estimated by mass-balance, seem rather high (e.g. Vielzeuf and Holloway, 1988) to explain the stability and abundance of biotite in a restitic assemblage such as that of the Grt–Bt–Sil xenoliths. The persistence of biotite at temperatures probably exceeding 850°C can be explained by the absence of quartz, that inhibited further melting, and by the high TiO_2 content of biotite, that expands the stability field of this mineral to higher temperatures (Patiño Douce and Johnston, 1991).

Regional implications

The xenoliths show evidence that intense deformation (i.e. foliation development) accompanied anatexis and melt extraction. Thus, the anatectic event is not the result of contact metamorphism induced by the dacitic magma, but is likely to reflect a process that was active on a regional scale.

Dacitic to andesitic rocks rich in metapelitic xenoliths comparable to those of El Joyazo are widespread in a large area from Mazarron to the Mar Menor, suggesting that the anatectic process was regional in scale. Our estimated P–T conditions indicate depths of about 20 km for anatexis/

TABLE 5. Results of the thermobarometric calculations

	Grt-Bt-Sil xenoliths				Spl-Crd xenoliths		
	HO33	SP 823	SP 829	SP 819D	HO 19	HO 27	HO 31
Temperature (°C)							
Grt-Bt Ferry and Spear, 1978	800–900	815	810	850–900	850–900	980	800
Pressure (kbar)							
GASP Newton and Haselton, 1981*	5.0–7.0	5.5–6.5	3.5–5.0		5.5–7.0		4.0–5.5
Grt-Crd Aranovich and Podlesskii, 1983		5.2–5.5	5.1–5.5	5.3–6.0	6.5	6.5–7.5	

* due to the absence of quartz, these values represent minimum pressures.

metamorphism, and average thermal gradients higher than 40°C/km. These values are in agreement with the present-day pronounced thermal anomaly, which is supposed to have been present since the Miocene, and with the calculated crustal thickness in this area (De Larouzière *et al.*, 1988). The high thermal gradients may have been achieved by uprise of hot mantle during regional crustal thinning and/or by emplacement, at the base of the crust, of large bodies of calc-alkaline basic magmas, the same magmas that generated the widely exposed calc-alkaline volcanic belt of the Cabo de Gata – Carboneras area and which occur as basaltic to gabbroic enclaves in the El Joyazo and similar dacites or andesites.

Conclusions

The metapelitic xenoliths in the dacite of El Joyazo represent restites after extraction of about 40–50 wt.% rhyolitic melt, part of which is still present as glass inclusions or melt pockets. The protolith of the xenoliths was probably a graphitic, fine grained metapelite, similar to those outcropping in the Alpujarride basement of the Betic Cordillera.

During partial melting and recrystallization of the metapelites, melt extraction was achieved mainly by flow along foliation planes, for minimum distances of about 20 cm, without collection into fracture networks. Melt extraction was assisted by intense ductile deformation, that produced the well-developed foliation in the xenoliths. Primary melt inclusions in the mineral phases involved in the fabric development confirm that the whole process took place during anatexis.

This natural example offers an exceptional insight, unaltered by later recrystallization and re-equilibration related to slow cooling, into the processes of crustal anatexis and magma segregation in a lithospheric extensional setting.

Acknowledgements

This paper benefitted from the reviews of J. Clemens, M. Holness and G. Stevens. We wish to thank G. Pennacchioni, F.P. Sassi and R. Spiess for discussion and critical reading of the manuscript. Financial support from Italian M.U.R.S.T. 40% and C.N.R. (grant 94.00788.CT05).

References

Aranovich, L.Ya. and Podlesskii, K.K. (1983) The cordierite-garnet-sillimanite-quartz equilibrium: experiments and applications. In *Kinetics and Equilibrium in Mineral Reactions* (S.K. Saxena, ed.) Springer, pp. 173–98.

Bellon, H., Bordet, P. and Montenat, C. (1983) Chronologie du magmatisme Nèogéne des Cordilléres Bètiques (Espagne Mèridionale). *Bull. Soc. Géol. France*, **25**, 205–17.

De Larouzière, F.D., Bolze, J., Bordet, P., Hernandez, J., Montenat, C. and Ott d'Estevou, P.(1988) The Betic segment of the lithospheric Trans-Alboran shear zone during the late Miocene. *Tectonophysics*, **152**, 41–52.

Di Battistini, G., Toscani, L., Iaccarino, S. and Villa, I.M. (1987) K/Ar age and the geological setting of calc-alkaline volcanic rocks from Sierra de Gata, SE Spain. *Neues Jahrb. Mineral. Mh.*, 369–83.

Ferry, J.M. and Spear, F.S. (1978) Experimental calibration of the partitioning of Fe and Mg between biotite and garnet. *Contrib. Mineral. Petrol.*, **66**, 113–7.

Grant, J.A. and Frost, B.R. (1990) Contact metamorphism and partial melting of pelitic rocks in the aureole of the Laramie Anorthosite Complex, Morton Pass, Wyoming. *Amer. J. Sci.*, **290**, 425–72.

Hayob, J.L., Essene, E.J., Ruiz, J., Ortega-Gutierrez, F. and Aranda-Gomez, J.J. (1989) Young high-temperature granulites from the base of the crust in central Mexico. *Nature*, **342**, 265–8.

Holtz, F. and Johannes, W. (1991) Genesis of peraluminous granites. I. Experimental investigation of melt compositions at 3 and 5 kb and various H_2O activities. *J. Petrol.*, **32**, 935–58.

Johnston, A.D. and Wyllie, P.J. (1988) Constraints on the origin of Archaean trondhjemites based on phase relationships of Nûk gneiss with H_2O at 15 kbar. *Contrib. Mineral. Petrol.*, **100**, 35–46.

Lopez-Ruiz, J. and Rodriguez-Badiola, E. (1980) La region volcanica Neogena del sureste de Espana. *Estudios Geologicos*, **36**, 5–63.

Munskgaard, N.C. (1984) High $\delta^{18}O$ and possible pre-eruptional Rb-Sr isochrons in cordierite-bearing Neogene volcanics from SE Spain. *Contrib. Mineral. Petrol.*, **87**, 351–8.

Munskgaard, N.C. (1985) A non-magmatic origin for compositionally zoned euhedral garnet in silicic Neogene volcanics from SE Spain. *Neues Jahrb. Mineral. Mh.*, 73–82.

Newton, R.C. and Haselton, H.T. (1981) Thermodynamics of garnet-plagioclase-Al_2SiO_5-quartz geobarometer. In *Thermodynamics of Minerals and Melts* (R.C. Newton, A. Navrotsky and B.J. Wood, eds.) Springer, pp. 131–47.

Nobel, F.A., Andriessen, P.A.M., Hebeda, E.H., Priem, H.N.A. and Rondeel, H.E. (1981) Isotopic dating of the post-Alpine Neogene volcanics in the Betic Cordilleras, Southern Spain. *Geol. Mijnbouw*, **60**, 209–14.

Patiño Douce, A. and Johnston, D.A. (1991) Phase equilibria and melt productivity in the pelitic system: implications for the origin of peraluminous granitoids. *Contrib. Mineral. Petrol.*, **107**, 202–18.

Roedder, E. (1984) Fluid inclusions. In *Reviews in Mineralogy*, **12**, 646pp.

Salvioli Mariani, E., Cesare, B. and Venturelli, G. (1995) Petrology of metapelite-derived xenoliths in the Hoyazo dacite (SE Spain). *Terra Abstracts*, **7**, 317.

Srogi, L., Wagner, M.A. and Lutz, T.M. (1993) Dehydration partial melting and disequilibrium in the granulite-facies Wilmington Complex, Pennsylvania-Delaware Piedmont. *Amer. J. Sci.*, **293**, 4O5–62.

Toscani, L., Venturelli, G., Barbieri, M., Capedri, S., Fernandez-Soler, J.M. and Oddone, M. (1990) Geochemistry and petrogenesis of two-pyroxene andesites from Sierra de Gata (SE Spain). *Mineral. Petrol.*, **41**, 199–213.

Vielzeuf, D. and Holloway, J.R. (1988) Experimental determination of the fluid-absent melting reactions in the pelitic systems. Consequences for crustal differentiation. *Contrib. Mineral. Petrol.*, **98**, 257–76.

Vielzeuf, D. and Montel, J.M. (1994) Partial melting of metagreywackes. Part 1. Fluid-absent experiments and phase relationships. *Contrib. Mineral. Petrol.*, **117**, 375–93.

Zeck, H.P. (1968) *Anatectic origin and further petrogenesis of almandine-bearing biotite-cordierite-labradorite dacite with many inclusions of restite and basaltoid material, Cerro de Hoyazo, SE Spain.* PhD Thesis, Amsterdam, 161 pp.

Zeck, H.P. (1970) An erupted migmatite from Cerro de Hoyazo, SE Spain. *Contrib. Mineral. Petrol.*, **26**, 225–46.

[*Manuscript received 27 October 1995: revised 12 June 1996*]